Supplement of Atmos. Chem. Phys., 25, 13831–13848, 2025
https://doi.org/10.5194/acp-25-13831-2025-supplement

Supplement of

Impact of atmospheric turbulence on the accuracy of point source emission estimates using satellite imagery

Michał Gałkowski et al.

Correspondence to: Michał Gałkowski (michal.galkowski@bgc-jena.mpg.de)

S1 Detailed WRF configuration

Table S1 contains information on the configuration of the model used in the experiment.

Table S1. Details of WRF-GHG model configuration.

	Basic information		
Domain codes	d01	d02	d03
Resolution	10 km x 10 km	2 km x 2 km	0.4 km x 0.4 km
Vertical resolution	85 full-model levels, 38 below 3 km a.g.l.		
Model top	50 hPa, approximately 20 km a.m.s.l.		
Time step	50 s	10 s	2 s
Feedback option	off		
	Parameterizations		
Microphysics	Thompson et al. (2004)		
Longwave radiation	RRTMG (Iacono et al., 2008)		
Shortwave radiation	RRTMG (Iacono et al., 2008)		
Surface layer	Revised MM5 (Jiménez et al., 2012)		
Land surface model	Noah LSM (Chen and Dudhia, 2001)		
Cumulus parameterization	GD (Grell and Dévényi, 2002)	off	off
PBL scheme	Shin and Hong (2015)		
Land use maps	MODIS 30" with lakes		
Elevation	GMTED 30"		
	Nudging		
On/off	on, to ECMWF HRES	off	off
Variables	wind, T, q[a]		
Interval	180 min		
Wind nudging levels	all levels		
Wind nudging coeff.	3.0×10^{-4} s^{-1}		
T nudging levels	$>=$ 40 (above 3 km)		
T nudging coeff.	3.0×10^{-4} s^{-1}		
q nudging levels	$>=$ 40 (above 3 km)		
q nudging coeff.	4.5×10^{-5} s^{-1}		

[a] - Here q denotes water vapour mixing ratio, defined as kg of vapour per kg of dry air, in accordance with WRF naming convention.

S2 Emissions and mole fractions at emission point

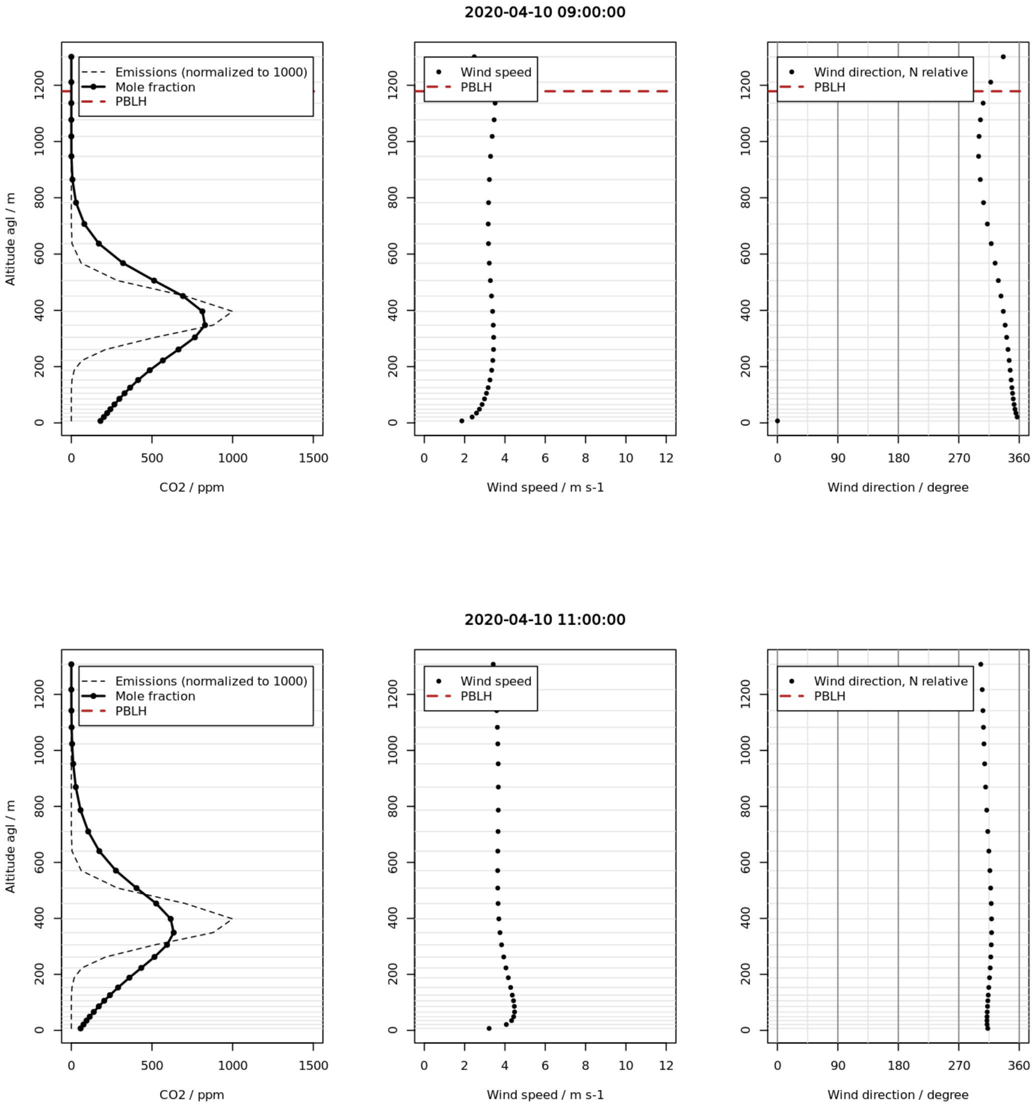

Figure S1. Vertical profiles of selected model variables at the emission point (Bełchatów Power Plant). Top: data from 09:00 UTC, 10 April 2020, extracted from WRF 400 m x 400 m output. Bottom: Same for 11:00 UTC. Left: CO_2 mole fractions in ppm (solid line). Vertical distribution of CO_2 emissions, normalized to 1000 (arbitrary units; dashed). Centre: wind speed (points) and Planetary Boundary Layer Height (PBLH, red, dashed). Right: wind direction and PBLH.

S3 Dry-air mole fractions of CO_2 tagged tracers (puffs)

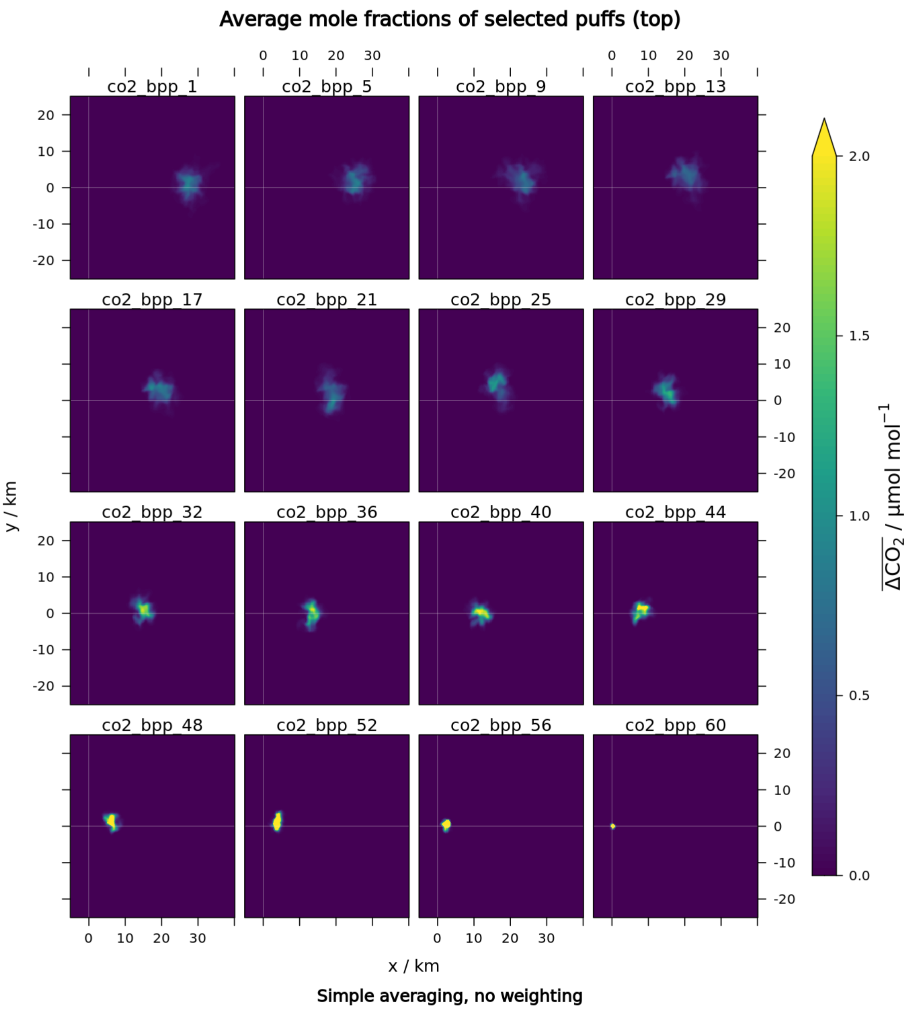

Figure S2. Average mole fraction of the temporally-tagged CO_2 tracers (puffs) at 12:00 UTC. Simple vertical averaging of mole fractions are presented. Effects of the gradual dispersion of the plume emitted at the power plant (located at $x = 0$, $y = 0$) is visible, with old tracers (e.g. co2_bpp_1 emitted between 09:00 – 09:03 UTC) spreading spatially as they move along the mean wind direction (increasing x). The final tracer, co2_pbb_60 was emitted between 11:57 – 12:00 UTC and the emitted mass is still in the direct vicinity of the source.

S4 Tracer mass discrepancies in the analysis area

In order to test whether the sum of individual tagged tracers (i.e. puffs) can be used to quantifiably interpret the emitted CO_2 plume, we have compared column-integrated values of the sum of puffs to a classical, reference tracer. As can be seen in Fig. S4, for the analysis area discussed in the study, namely 2–22 km range, local discrepancies caused by high local gradients occur only in the immediate vicinity of the emission source and are affecting the mass distribution locally at distances lower than 5 km. However, the total mass of the emitted plume is well preserved in both cases, with two versions of the plume carrying mass identical within 0.035 %.

We conclude that for the purposes of this study, both tracers can be treated as identical.

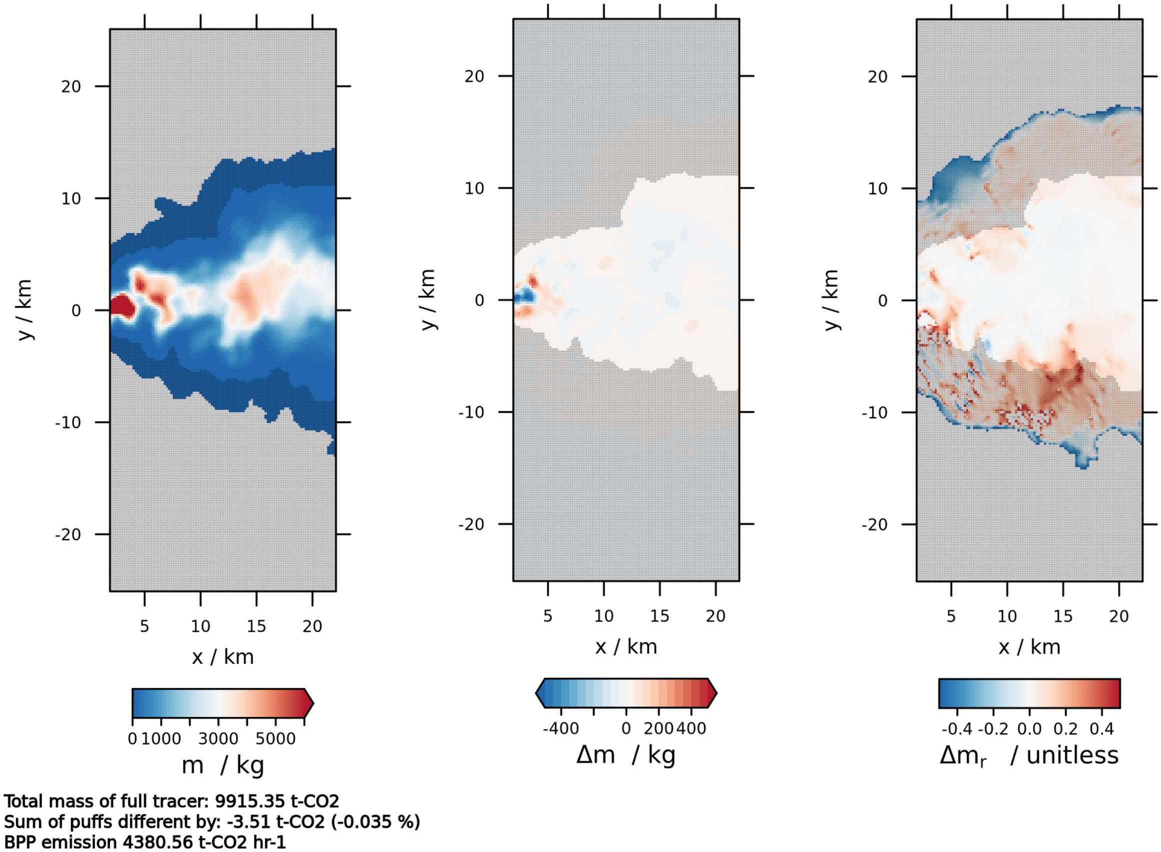

Figure S3. Left: Total column integrated mass of CO_2. Middle: mass discrepancy in the analysis area (2–22 km between the sum of 60 temporally-tagged tracers (co2_bpp_1 to co2_bpp_60) and the full tracer signal (reference) caused by the model's mass-conserving advection scheme. Right: relative pointwise mass discrepancy ($\Delta m/m$). Relative mass discrepancy integrated over the area shown is 0.35 ‰. Shaded areas in the figure panels contain 10^{-4} of the total tracer mass in the presented spatial extent.

References

Chen, F. and Dudhia, J.: Coupling an Advanced Land Surface–Hydrology Model with the Penn State–NCAR MM5 Modeling System. Part I: Model Implementation and Sensitivity, Monthly Weather Review, 129, 569 – 585, https://doi.org/10.1175/1520-0493(2001)129<0569:CAALSH>2.0.CO;2, 2001.

Grell, G. A. and Dévényi, D.: A generalized approach to parameterizing convection combining ensemble and data assimilation techniques, Geophysical Research Letters, 29, 38–1–38–4, https://doi.org/https://doi.org/10.1029/2002GL015311, 2002.

Iacono, M. J., Delamere, J. S., Mlawer, E. J., Shephard, M. W., Clough, S. A., and Collins, W. D.: Radiative forcing by long-lived greenhouse gases: Calculations with the AER radiative transfer models, Journal of Geophysical Research: Atmospheres, 113, https://doi.org/https://doi.org/10.1029/2008JD009944, 2008.

Jiménez, P. A., Dudhia, J., González-Rouco, J. F., Navarro, J., Montávez, J. P., and García-Bustamante, E.: A Revised Scheme for the WRF Surface Layer Formulation, Monthly Weather Review, 140, 898 – 918, https://doi.org/10.1175/MWR-D-11-00056.1, 2012.

Shin, H. H. and Hong, S.-Y.: Representation of the Subgrid-Scale Turbulent Transport in Convective Boundary Layers at Gray-Zone Resolutions, Monthly Weather Review, 143, 250 – 271, https://doi.org/10.1175/MWR-D-14-00116.1, 2015.

Thompson, G., Rasmussen, R. M., and Manning, K.: Explicit Forecasts of Winter Precipitation Using an Improved Bulk Microphysics Scheme. Part I: Description and Sensitivity Analysis, Monthly Weather Review, 132, 519 – 542, https://doi.org/10.1175/1520-0493(2004)132<0519:EFOWPU>2.0.CO;2, 2004.